THE ASTROPHYSICAL JOURNAL, 474:315–328, 1997 January 1

LOCAL INTERSTELLAR MEDIUM PROPERTIES AND DEUTERIUM ABUNDANCES FOR THE LINES OF SIGHT TOWARD HR 1099, 31 COMAE, β CETI, AND β CASSIOPEIAE[1]

NIKOLAI PISKUNOV,[2] BRIAN E. WOOD,[3] JEFFREY L. LINSKY,[3]
ROBERT C. DEMPSEY,[4] AND THOMAS R. AYRES[5]

Received 1996 March 15; accepted 1996 July 24

ABSTRACT

We analyze Goddard High-Resolution Spectrograph data to infer the properties of local interstellar gas and the deuterium/hydrogen (D/H) ratio for lines of sight toward four nearby late-type stars—HR 1099, 31 Comae, β Ceti, and β Cassiopeiae. The data consist of spectra of the hydrogen and deuterium Lyα lines, and echelle spectra of the Mg II *h* and *k* lines toward all stars except β Cas. Spectra of the RS CVn–type spectroscopic binary system HR 1099 were obtained near opposite quadratures to determine the intrinsic stellar emission line profile and the interstellar absorption separately. Multiple-velocity components were found toward HR 1099 and β Cet. The spectra of 31 Com and β Cet are particularly interesting because they sample lines of sight toward the north and south Galactic poles, respectively, for which H I and D I column densities were not previously available.

The north Galactic pole appears to be a region of low hydrogen density like the "interstellar tunnel" toward ε CMa. The temperature and turbulent velocities of the local interstellar medium (LISM) that we measure for the lines of sight toward HR 1099, 31 Com, β Cet, and β Cas are similar to previously measured values ($T \approx 7000$ K and $\xi = 1.0$–1.6 km s^{-1}). The deuterium/hydrogen ratios found for these lines of sight are also consistent with previous measurements of other short lines of sight, which suggest D/H $\approx 1.6 \times 10^{-5}$. In contrast, the Mg abundance measured for the β Cet line of sight [implying a logarithmic depletion of D(Mg) $= +0.30 \pm 0.15$] is about 5 times larger than the Mg abundance previously observed toward α Cen, and about 20 times larger than all other previous measurements for the LISM. These results demonstrate that metal abundances in the LISM vary greatly over distances of only a few parsecs.

Subject heading: binaries: spectroscopic — ISM: abundances — ISM: clouds — ultraviolet: ISM

1. INTRODUCTION

The echelle gratings and Digicon detectors in the *Hubble Space Telescope's* (*HST*) Goddard High-Resolution Spectrograph (GHRS) make the GHRS an excellent instrument for studying narrow absorption lines formed by the interstellar medium. With this instrument, one can obtain both high spectral resolution ($\lambda/\Delta\lambda \approx 86{,}000$; $\Delta v \approx 3.5$ km s^{-1}) and high signal-to-noise ratio (S/N). The use of the 0.″25 × 0.″25 small science aperture (SSA) suppresses geocoronal Lyα emission, provides a well-characterized instrumental profile with relatively little scattered light, and provides an accurate wavelength scale. For a description of the GHRS instrument, see Brandt et al. (1994) and Heap et al. (1995). Soderblom et al. (1994) have described the improved characteristics of the GHRS after the repair mission when the COSTAR optics were installed on the *HST*. Although interstellar lines in the ultraviolet were studied with the *Copernicus* and the *International Ultraviolet Explorer* (*IUE*) spacecraft, the superior properties of the GHRS provide the opportunity to address a whole new range of interstellar medium questions and to reexamine previously studied issues from a fresh perspective.

The analysis of GHRS echelle spectra of nearby stars has allowed us to address four important but closely interrelated questions. First, the dynamics and structure of the warm interstellar gas near the Sun (the so-called local interstellar medium or LISM) can be studied by measuring the velocities of interstellar absorption features along many lines of sight and by determining whether the absorption lines are composed of several velocity components. Lallement & Bertin (1992) and Lallement et al. (1995) concluded that nearly all lines of sight toward nearby stars show Mg II and Fe II absorption lines consistent with a flow vector in the heliocentric rest frame with a magnitude of 26 ± 1 km s^{-1} moving toward Galactic coordinates $l = 186° \pm 3°$ and $b = -16° \pm 3°$. This result, and the observation that neutral helium flowing through the heliosphere has about the same velocity vector, led Lallement & Bertin (1992) to conclude that the Sun is located inside a cloud (called the local interstellar cloud or LIC) that appears to move through the Galaxy as a rigid body and extends for several parsecs in some directions. The presence of additional discrete velocity components, even toward nearby stars like Sirius (2.7 pc), Procyon (3.5 pc), and Altair (5 pc), indicates that there are other warm interstellar clouds outside of the LIC. Linsky, Piskunov, & Wood (1996) have presented three-dimensional morphologies of the LIC and the total amount of gas in the LISM based on all of the

[1] Based on observations with the NASA/ESA *Hubble Space Telescope*, obtained at the Space Telescope Science Institute, which is operated by the Association of Universities for Research in Astronomy, Inc., under NASA contract NAS5-26555.

[2] Uppsala Astronomical Observatory, Box 515, S-75120 Uppsala, Sweden; piskunov@astro.uu.se.

[3] JILA, University of Colorado, Boulder, CO 80309-0440; woodb@marmot.colorado.edu, jlinsky@jila.colorado.edu.

[4] Astronomy Programs, Computer Sciences Corporation, Space Telescope Science Institute, 3700 San Martin Drive, Baltimore, MD 21218; dempsey@stsci.edu.

[5] Center for Astrophysics and Space Astronomy, University of Colorado, Boulder, CO 80309-0389; ayres@vulcan.colorado.edu.

TABLE 1

SUMMARY OF GHRS OBSERVATIONS

Start Time[a]	Proposal Number	Observation Identification	Grating Order	Central λ (Å)	Duration (s)	Aperture	Phase
HR 1099 = HD 22468 (K0 IV + G5 V) ($l = 185°$, $b = -41°$, $d = 36$ pc)							
1993 Sep 14 18:48	4873	Z1GT0202	G160M	1223	3917	SSA	0.24
1993 Sep 15 02:34	4447	Z1GV0806	EB-20	2800	109	LSA	0.34
1993 Sep 18 15:49	4447	Z1GV0C06	EB-20	2800	109	LSA	0.59
1993 Sep 19 01:16	4874	Z1GU0703	EB-22	2600	979	SSA	0.73
1993 Sep 19 17:43	4447	Z1GV0206	EB-20	2800	109	LSA	0.97
1993 Sep 21 21:02	4874	Z1GU0503	EB-20	2800	1414	SSA	0.73
1995 Jul 09 17:42	5733	Z2NG0108	EA-46	1215.7	3917	SSA	0.85
31 Com = HD 111812 (G0 III) ($l = 115°$, $b = +89°$, $d = 80$ pc)							
1994 Nov 07 20:33.....	5323	Z2DC010BT	G160M	1222.6	646	SSA	...
1994 Nov 07 19:10.....	5323	Z2DC0108T	EB-20	2797.7	1293	SSA	...
β Cet = HD 4128 (K0 III) ($l = 111°$, $b = -81°$, $d = 16$ pc)							
1994 Jun 02 21:25	5323	Z2DC020BT	G160M	1222.6	323	SSA	...
1994 Jun 02 21:13	5323	Z2DC0208T	EB-20	2797.8	323	SSA	...
β Cas = HD 432 (F2 III–IV) ($l = 118°$, $b = -3°$, $d = 14$ pc)							
1995 Nov 22 15:30.....	6067	Z2ZD010GT	G140M	1215	1414	SSA	...

[a] This first column lists the year, day of year, and Universal Time in hours and minutes at which each observation began.

published GHRS data and the *Extreme-Ultraviolet Explorer* (*EUVE*) spectra of hot white dwarfs.

Second, one would like to measure the physical properties of the LIC and the other nearby clouds, including such quantities as their temperature, density, degree of ionization, turbulence, shear, rotation, and magnetic field strength. High-resolution profiles of absorption lines of both low-mass (e.g., hydrogen and deuterium) and high-mass (e.g., Mg II and Fe II) ions along relatively simple lines of sight provide the opportunity to infer both the temperature and the nonthermal velocities (often called turbulence). Applying this technique to the Capella line of sight, which has only one velocity component, Linsky et al. (1993, hereafter Paper I) measured the temperature ($T = 7000 \pm 900$ K) and turbulence ($\xi = 1.6 \pm 0.6$ km s^{-1}) of the LIC. Both quantities include estimates of the systematic errors associated with the uncertain stellar intrinsic emission line profiles of the spectroscopic binary. Analysis of the Procyon line of sight by Linsky et al. (1995, hereafter Paper II) led to a similar temperature ($T = 6900 \pm 380$ K) but a somewhat smaller value for the turbulence ($\xi = 1.21 \pm 0.27$ km s^{-1}). On the other hand, the line of sight to α Cen A and α Cen B (Linsky & Wood 1996, hereafter Paper III), which passes through another cloud (the so-called Galactic or G cloud), is characterized by a lower temperature ($T = 5400 \pm 500$ K) but a turbulence value ($\xi = 1.20 \pm 0.25$ km s^{-1}) similar to that found for the Procyon line of sight through the LIC.

Third, one would like to measure the chemical composition and ionization in the local clouds, and especially the deuterium/hydrogen (D/H) ratio, which can be related to the primordial D/H ratio. The latter is an important constraint on models of the early universe, since it is a critical parameter for measuring the baryon density. An accurate determination of the D/H ratio is made difficult by (1) the unknown intrinsic stellar Lyα emission line against which the interstellar H and D absorption must be measured and (2) the very saturated H Lyα absorption. (Typical line-center optical depths are 10^5.) One way to minimize errors in the derived D/H ratio is to observe a spectroscopic binary system at opposite quadratures, so that the broad composite emission line produced by the two stars has a different shape and radial velocity at the two orbital phases, whereas the interstellar absorption should not change. Using this technique in Paper II, we were able to derive $D/H = 1.60^{+0.14}_{-0.19} \times 10^{-5}$ for the Capella line of sight. By comparison, analyses of the low radial velocity single stars Procyon (Paper II), α Cen A, and α Cen B (Paper III) led to D/H ratios consistent with this value, but with much larger uncertainties. Wood, Alexander, & Linsky (1996a, hereafter Paper IV) developed another technique for inferring the value of D/H toward the high radial velocity star ϵ Ind. The large Doppler shift between the star and the interstellar absorption permitted them to infer the H column density from the optically thin H absorption line wings rather than from the saturated core. They inferred $D/H = (1.6 \pm 0.4) \times 10^{-5}$ for this line of sight, and a similar value for the λ And line of sight. Thus, it now appears that the D/H ratio does not vary significantly with location in the LISM, but more lines of sight must be studied to verify this tentative result.

Fourth, interesting physical processes occur when the inflowing, partially ionized interstellar gas interacts with the ionized hot wind of the Sun and other stars. Theoretical studies (e.g., Baranov & Malama 1995; Williams et al. 1997; Pauls, Zank, & Williams 1995), which include charge-exchange interactions between the inflowing hydrogen atoms and the outflowing solar wind protons, predict that, near the heliopause, there should be a region of higher density, warm, decelerated neutral hydrogen called the "hydrogen wall." In Paper III, Linsky & Wood observed additional absorption on the long-wavelength side of the interstellar hydrogen absorption toward α Cen A and α Cen B, which they concluded is absorption by the hydrogen wall gas around the Sun. They found that neutral hydrogen in the wall has a temperature of $T = 29{,}000 \pm 5000$ K, a

column density of $\log N_{\rm H\,I} = 14.74 \pm 0.24$ cm^{-2}, and a velocity about 4 km s^{-1} slower than the interstellar inflow velocity. As detailed in Paper IV, Wood et al. discovered hotter hydrogen walls around the stars ϵ Ind and λ And, with the higher temperatures probably resulting from the larger velocity differences between the interstellar gas and the stellar motion.

These four major questions cannot be addressed in isolation. For example, the presence of several velocity components must be included when analyzing the line profile shapes, in order to infer the temperature of the LISM and the D/H ratio. Also, the presence of hydrogen walls around the Sun and stars can change the apparent shape of the interstellar absorption, and thus change the inferred D/H ratio by a factor of 2.

In this paper, the fifth in our series, we analyze the GHRS spectra of four stars in order to answer the first three questions for the LISM gas along new lines of sight. We will analyze echelle spectra of the Lyα, Mg II, and Fe II lines toward the RS CVn–type spectroscopic binary system HR 1099 (G5 IV + K1 IV). Near one quadrature (phase 0.85), we have an echelle spectrum of the Lyα line, but near the opposite quadrature (phase 0.24), we have a lower resolution ($\lambda/\Delta\lambda \approx 16{,}000$; $\Delta v \approx 18.75$ km s^{-1}) G160M spectrum of this line. We also analyze G160M spectra of 31 Comae (G0 IIIp) and β Ceti (K0 III), and a G140M spectrum of β Cassiopeiae (F2 III–IV), which has a resolution of $\lambda/\Delta\lambda \approx 21{,}000$ and $\Delta v \approx 14.3$ km s^{-1}. Although the spectra for the latter three stars were obtained primarily for other purposes and are not ideal for interstellar studies, they do provide useful interstellar data with somewhat lower accuracy than the HR 1099 data. Also, these three stars sample the LISM along previously unexplored lines of sight, including both Galactic poles. The Galactic coordinates of the stars are listed in Table 1.

In addition to the lines of sight previously mentioned, the GHRS also has been used to study the lines of sight toward G191-B2B (Lemoine et al. 1996), Sirius (Lallement et al. 1994), α PsA (Ferlet et al. 1995), Altair, Vega, β Pic, δ Cas (Lallement et al. 1995), and ϵ CMa (Gry et al. 1995).

2. GHRS OBSERVATIONS

Table 1 summarizes the circumstances of the GHRS observations of the four stars. The data were obtained under six observing programs (listed in the second column of the table) with principal investigators J. L. Linsky (programs 4873, 4874, and 5733), R. C. Dempsey (program 4447), and T. R. Ayres (programs 5323 and 6067). The first column of the table lists the year, day of year, and Universal Time in hours and minutes at which each observation began. The data for HR 1099 were obtained on 1993 September 14–21 and 1995 July 9. The data for the other stars were obtained on 1994 June 2, 1994 November 11, and 1995 November 22. The remaining columns of the table contain the observation identification (useful for accessing the data in the *HST* archive), the grating and echelle order number (EA and EB refer to the short- and long-wavelength echelles, respectively), the central wavelength of each spectrum, the effective integration time, and the orbital phase (for HR 1099). Table 1 lists observations obtained through the SSA and those obtained through the large science aperture (LSA). The data were processed with the version of CALHRS software available in 1995. The EA data for HR 1099 were obtained by using the FP-SPLIT mode to reduce the fixed-pattern noise. The individual readouts of the FP-SPLIT spectra were combined by using a cross-correlation procedure called HRS_MERGE (Robinson et al. 1992). Images of the Pt-Ne calibration lamp, taken prior to or immediately following all of the observations, were used to calibrate the wavelengths of the spectra.

3. ANALYSIS OF THE LINE OF SIGHT TOWARD HR 1099

HR 1099 (= V711 Tau = HD 22468) is a double-lined RS CVn–type spectroscopic binary system (K1 IV and G5 IV) with a very high level of activity. The stellar components have masses of 1.4 and 1.1 $M_\odot$ with radii of 3.9 and 1.3 $R_\odot$, respectively. The orbital period is 2.84 days, and the system is located 36 pc from the Sun (Strassmeier et al. 1993). The projected radial velocities vary with amplitudes of 62.8 (K1 star) and 50 (G5 star) km s^{-1}, and the γ velocity is -15.4 km s^{-1} (Donati et al. 1992).

Photometric observations of HR 1099 revealed the presence of a complex pattern of cold spots in the stellar photospheres (Henry et al. 1995), which change with time. Doppler and Zeeman-Doppler maps of the photosphere of the primary have been generated by using optical spectroscopy (Vogt 1988; Donati et al. 1992).

Using *IUE* observations of HR 1099, Ayres & Linsky (1982) found that the K star produces most of the UV emission in the system. HR 1099 has a very high X-ray luminosity, $\log L_{\rm X} = 31.38$ (Dempsey et al. 1993), and shows many other signatures of high activity, including strong Lyα and Mg II *h* and *k* emission. Both Lyα and Mg II *h* and *k* emission provide bright background "continua" against which to analyze interstellar absorption lines. Observations at different orbital phases, especially near quadratures where the orbital Doppler shifts are largest, may provide the information required to infer the intrinsic emission line profiles.

Several sets of GHRS observations of HR 1099 were available for this work. The Mg II *h* and *k* lines were observed with the EB grating at four phases: 0.34, 0.59, 0.73, and 0.97 (Fig. 1). The phase 0.73 spectrum (Fig. 1*c*), which has a much higher S/N because of its longer exposure time (see Table 1), was selected as the primary data set for our analysis. The stellar Mg II lines in the spectrum were analyzed in detail by Wood et al. (1996b). Dempsey et al. (1996) have discussed the variability of the Mg II profiles present in the entire data set.

Lyα profiles where obtained at phases 0.24 and 0.85 by using the G160M and EA gratings, respectively (Fig. 2). The spectra at both phases show broad interstellar H I absorption centered at 1215.8 Å and a much narrower D I line centered at 1215.4 Å. Geocoronal emission present in the middle of the interstellar H I absorption line was fitted with a Gaussian and subtracted from the data. We also subtracted scattered light (1.3×10^{-13} ergs cm^{-2} s^{-1} Å^{-1} for the G160M spectrum and 4.7×10^{-13} ergs cm^{-2} s^{-1} Å^{-1} for the EA spectrum) as the interstellar H I opacity completely absorbs all of the stellar flux at line center. Unfortunately, the radial velocity variation amplitude for HR 1099 ($\approx$113 km s^{-1}) is not sufficient to shift the Lyα emission of the two stellar components completely out of the saturated interstellar core. We also see indications of a change in the intrinsic profile between the two exposures, which is not surprising considering the high level of activity in the system. We have therefore adopted the following method of analysis:

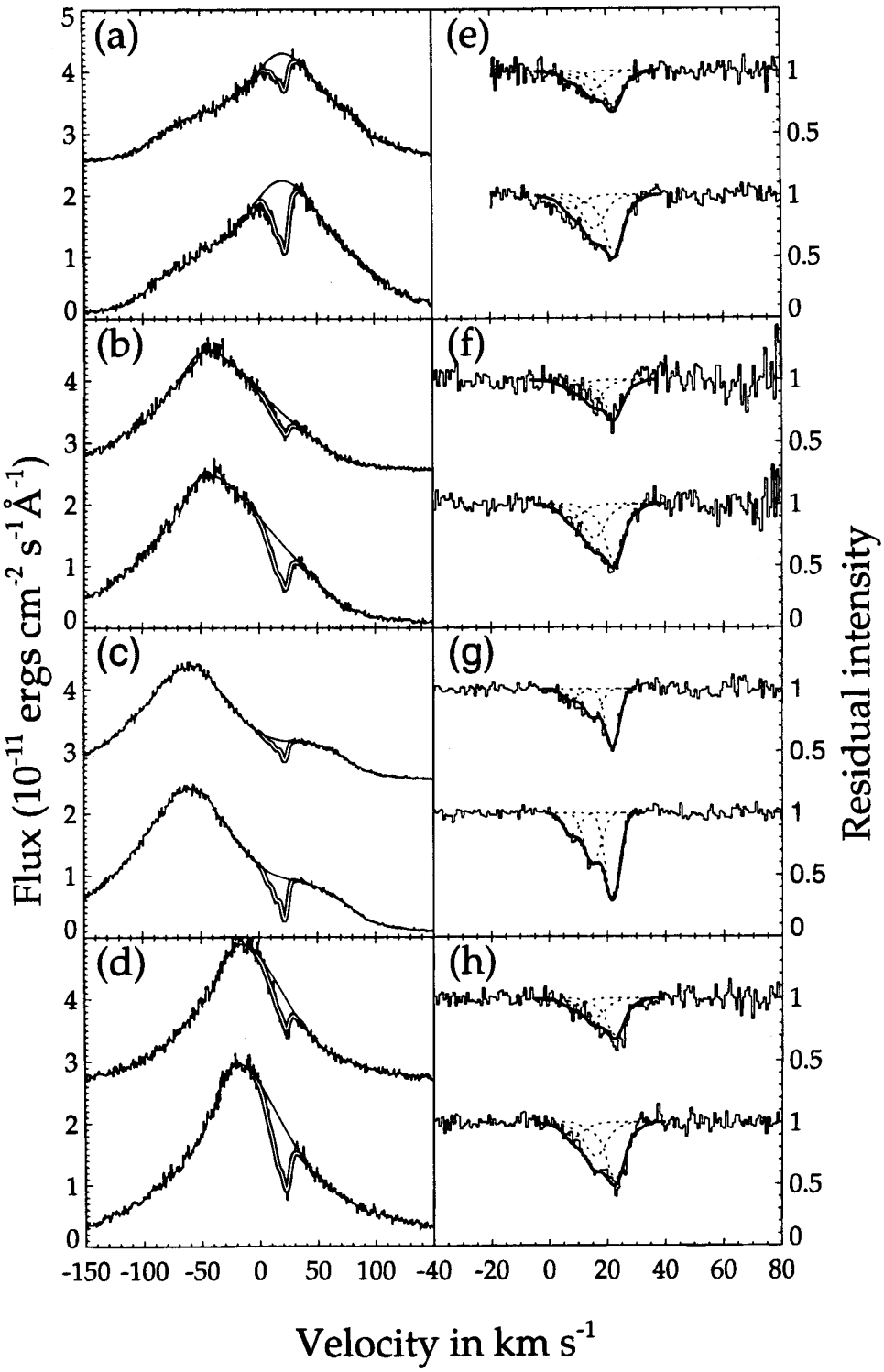

FIG. 1.—The three-component fit to the ISM absorption in Mg II *h* and *k* lines toward HR 1099 in the heliospheric rest frame. In each panel, the *h* line is on the top. *Left panels*: the original data for phases (*a*) 0.36, (*b*) 0.59, (*c*) 0.73, and (*d*) 0.97. *Smooth solid lines*: our reconstruction of the intrinsic profile. *Double lines*: our model of the ISM absorption. *Right panels*: the ISM profiles normalized by intrinsic stellar emission. *Dashed lines*: the individual ISM components, and the thick solid line represents the total absorption.

1. Use the Mg II *h* and *k* lines to determine the number of velocity components of the interstellar medium (ISM) absorption and to derive their velocities, line widths, and column densities.

2. Apply the ISM absorption parameters obtained from the Mg II lines to Lyα in order to derive the interstellar H I column density and the D/H ratio, with reasonable assumptions about the intrinsic stellar emission line profile.

3.1. Mg II *h and k Interstellar Absorption*

The relatively small optical depth and thermal width of the interstellar Mg II *h* and *k* lines make them very suitable for identifying ISM absorption components. We analyzed the phase 0.73 spectrum (Fig. 1*c*) because of its high S/N, the use of the SSA to achieve the best resolution, and the location of the interstellar absorption on a nearly horizon-

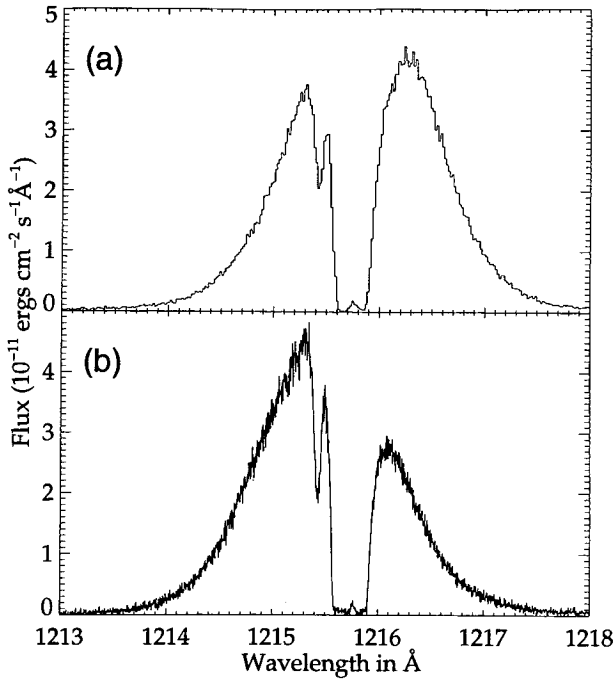

FIG. 2.—The original GHRS observations of Lyα profiles of HR 1099 in the rest frame of the Sun: (*a*) G160M observation at phase 0.24; (*b*) EA observation at phase 0.85. Geocoronal emission is visible in the middle of a broad absorption by interstellar hydrogen.

tal portion of the emission profile. We reconstructed the intrinsic profile of Mg II *h* and *k* lines by fitting fifth-order polynomials to the data points in the intervals (−40 km s^{-1}, −10 km s^{-1} and +32 km s^{-1}, +80 km s^{-1}). The interstellar profiles of the *h* and *k* lines were fitted simultaneously with multiple Gaussians by using nonlinear least-squares optimization (Bevington & Robinson 1992). The shape of the ISM absorption suggests the presence of more than one velocity component. Our attempt to make a two-component fit failed because it required an unrealistically large Doppler parameter of one of the components. The three-component fit (Fig. 1) gives satisfactory results in terms of the residual χ^2 value and parameter range. Table 2 lists the derived parameter values (central velocities, Doppler parameters [*b*], and Mg II column density [$N_{\rm Mg\,II}$]), together with random errors estimated by Monte Carlo techniques. Figure 1 shows that the parameters of the fit, derived for phase 0.73, lead to good agreement with other observations.

3.2. *Hydrogen and Deuterium Lyα Interstellar Absorption*

The major problem in deriving interstellar column densities for H I and D I from the Lyα profile is the unknown intrinsic shape of the stellar emission line. Even though the epochs of our GHRS observations were selected such that the stellar emission from both stars has maximum Doppler shifts relative to the interstellar line, the width of the saturated H I absorption is so large that part of the intrinsic stellar profile can never be observed. In addition, one expects that such a highly active object as HR 1099 will have spatially inhomogeneous and time-variable Lyα emission. It is also not clear whether the G star contributes significantly to the total Lyα flux.

We deal with these complications by using Ockham's razor (Ockham, ca 1320), starting with the simplest assumption and adding more complexity (if not realism) to our model until we can reproduce the observations.

For the two stars of the Capella binary system and for the G8 III star δ Lep, there appears to be a strong similarity between the Mg II *h* and *k* line profiles and the Lyα profiles, when the profiles are compared on the same wavelength scale rather than on the same velocity scale (Neff et al. 1990; Ayres et al. 1993). We found that the same empirical rule holds for HR 1099, except that the contribution of the G star is clearly visible in the Mg II lines but not Lyα (see Wood et al. 1996b). We therefore started our analysis by assuming that the intrinsic Lyα profile has the same shape as the Mg II *k* line. The two observed Lyα profiles of HR 1099 (Fig. 2) contain different total fluxes with about 15% more flux at phase 0.24 (Fig. 2*a*), even though the ISM line is better centered on the stellar emission. This finding suggests that the intrinsic profile varies with phase or time. We therefore allowed our χ^2 minimization procedure to scale the intrinsic profiles of each star in flux differently for the two phases while keeping the profile shapes the same. The best fit is achieved by scaling the intrinsic profile at phase 0.24 by 1.19 ± 0.002 relative to the profile at phase 0.85. For each of the three ISM components, we used the same velocities as determined from Mg II and included the two fine-structure components (separation 1.33 km s^{-1}) of the H I and D I lines (as described in Paper I). The free parameters included the H I column density, the D/H ratio, the Doppler widths, and the relative strengths of the three velocity components. We assumed the same D/H ratio for all of the ISM components. The resulting fit was far from perfect. Our next step was to include the G star contribution by using the same shape but different scaling factors. Since the improvement of the fit was marginal, we returned to the question of the intrinsic shape of Lyα emission; again we ignored the contribution of the G star. This time we allowed our code to search for the shape of the intrinsic stellar Lyα emission line, and we restricted only the curvature of the profile. The

TABLE 2

PARAMETERS FOR THE Mg II INTERSTELLAR LINES

Star	Figure	Velocity (km s^{-1})	$b_{\rm Mg\,II}$ (km s^{-1})	log $N_{\rm Mg\,II}$	χ^2_ν
HR 1099.....	1	21.9 ± 0.06	2.61 ± 0.09	12.12 ± 0.01	1.041
		14.8 ± 0.07	2.42 ± 0.08	11.74 ± 0.02	1.041
		8.2 ± 0.10	3.19 ± 0.10	11.49 ± 0.08	1.041
31 Com.....	6	−3.5 ± 0.1	2.39 ± 0.10	12.514 ± 0.010	1.037
β Cet.....	8	9.1 ± 0.1	2.46 ± 0.08	14.245 ± 0.104	1.952
		1.6 ± 0.1	3.71 ± 0.10	12.668 ± 0.020	1.952
β Cet.....	9	(9.1)	(2.46)	(14.245)	2.442
		3.4 ± 0.3	(2.46)	12.425 ± 0.026	2.442
		−0.4 ± 0.1	(2.46)	12.326 ± 0.031	2.442

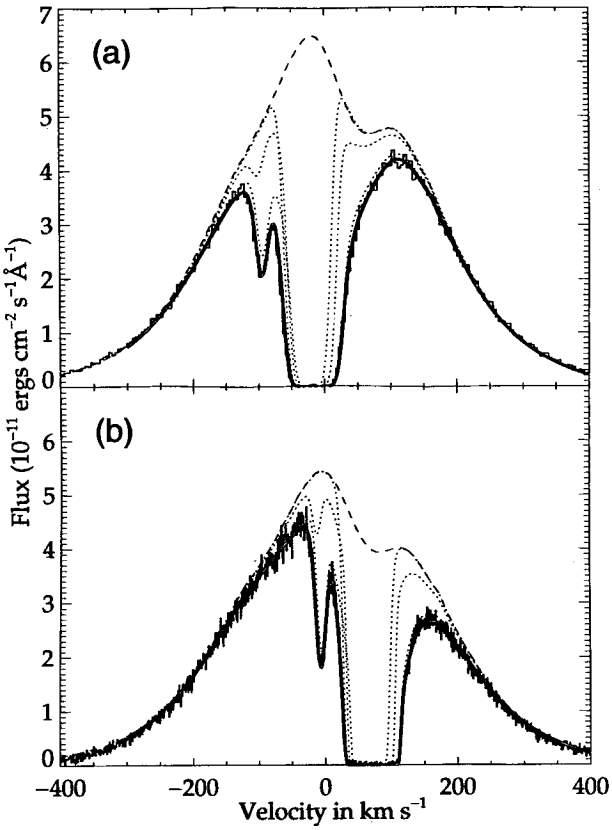

FIG. 3.—Best fit of the Lyα profiles for phase 0.24 (*a*) and 0.85 (*b*). The velocity scale is the rest frame of the K star. The dashed lines are the intrinsic stellar profiles, the dotted lines are individual absorption components, and the double lines are the combination of the intrinsic profile and total ISM absorption.

problem remains well constrained because the same shape for the stellar emission line was used to fit both phases. We also allowed the code to adjust the Doppler shift of the intrinsic profile. The best fit was achieved by shifting the intrinsic profile by -14.2 ± 0.1 km s^{-1} relative to its predicted position at phase 0.24. In this case, we obtained the very good fit shown in Figure 3. Numerical experiments confirmed the uniqueness of the solution, given the assumptions described above. Nonthermal velocity values were determined individually for each component by comparing the Doppler widths for H I and Mg II and assuming that both interstellar features are formed at the same temperature.

In order to estimate errors of the derived parameters, we followed two different approaches. First, we used Monte Carlo techniques to find the random errors, which turned out to be quite small. Most of the systematic errors are related to the selected shape of the intrinsic Lyα profile. Our model ignores a possible contribution from the G star and a time variation of the shape of the intrinsic profile. In addition, there are systematic errors associated with the derivation of the shape of Lyα. We estimated those errors by altering and fixing the intrinsic profile and recomputing the other parameters. Table 3 contains the list of free parameters and our estimate of the sum of the random and systematic errors.

The final parameters for the HR 1099 line of sight (Table 3) for the radial velocity, temperature, and D/H ratio are consistent with the parameter values for the other directions in the LIC. Even more reassuring is the result that the relative contributions of the three interstellar components, derived mainly from the D I line (14%, 25%, 60%), are very close to those determined from the Mg II *h* and *k* lines (11%, 29%, 59%). The 19% change of the Lyα flux and the 14.2 km s^{-1} shift of the intrinsic stellar line profile could result from an inhomogeneous distribution of emission regions on the surface of HR 1099.

4. OBSERVATIONS OF 31 COM, β CET, AND β CAS

We have obtained moderate-resolution spectra of the Lyα lines of 31 Com, β Cet, and β Cas. For 31 Com and β Cet, we also have high-resolution EB spectra of the Mg II *h* and *k* lines at 2802.705 Å and 2795.528 Å, respectively. The

TABLE 3

SUMMARY OF FINAL PARAMETERS FOR THE INTERSTELLAR ABSORPTION COMPONENTS

STAR	V (km s^{-1}) Observed	V (km s^{-1}) LIC	b_{HI} (km s^{-1})	T (10^3 K)	ξ (km s^{-1})	log N_{HI}	D/H (10^{-5})	D/Mg II	D(Mg)
HR 1099	21.9 ± 2	23.4	11.5 ± 1.0	7.8 ± 1.6	1.2 ± 0.2	17.9 ± 0.05	1.46 ± 0.09	8.8 ± 1.9	-1.36 ± 0.15
	8.2 ± 2	23.4	11.1 ± 1.0	7.3 ± 1.5	1.6 ± 0.7	17.2 ± 0.10	(1.46 ± 0.09)	7.0 ± 1.3	-1.29 ± 0.18
	14.8 ± 2	23.4	13.6 ± 1.2	11.1 ± 2.4	0.7 ± 0.2	17.6 ± 0.08	(1.46 ± 0.09)	10.5 ± 1.7	-1.44 ± 0.16
31 Com	-4 ± 1	−7.1	11.1 ± 1.3	7.5 ± 1.8	<1.5	17.95 ± 0.15	1.5 ± 0.4	4.7 ± 0.5	-1.03 ± 0.15
β Cet	8 ± 2	8.2	10.3 ± 2.2	6.6 ± 2.9	<2.0	18.35 ± 0.10	2.2 ± 1.1	0.35 ± 0.25	$+0.30 \pm 0.15$
	1 ± 2	8.2	14.5 ± 1.5	12.7 ± 2.7	2.2 ± 0.6	16.77 ± 0.20	(2.2 ± 1.1)	(0.35 ± 0.25)	$(+0.30 \pm 0.15)$
β Cas	10 ± 1	9.5	11.0 ± 2.0	7.0 ± 3.0	...	18.18 ± 0.13	1.6 ± 0.4	...	...
Capella	22.0 ± 0.9	22.0	10.87 ± 0.28	7.0 ± 0.9	1.6 ± 0.6	18.24 ± 0.05	$1.60^{+0.14}_{-0.19}$	4.1 ± 0.4	-1.07 ± 0.05
Procyon[a]	20.8 ± 1.5	19.8	10.83 ± 0.15	6.9 ± 0.38	1.21 ± 0.27	17.88 ± 0.05	(1.6 ± 0.2)	5.2 ± 0.7	-1.11 ± 0.05
α Cen[b]	-18.0 ± 0.2	−15.7	9.5 ± 0.2	5.4 ± 0.5	1.20 ± 0.25	17.59 ± 0.05	(1.6 ± 0.2)	1.2 ± 0.2	-0.46 ± 0.05
ε Ind.....	-9.2 ± 1.0	−8.9	11.9 ± 0.3	8.5 ± 0.5	(1.2)	18.0 ± 0.1	1.6 ± 0.4	...	...
λ And.....	6.5 ± 1.0	7.6	13.8 ± 0.3	11.5 ± 0.5	(1.2)	18.45 ± 0.15	1.7 ± 0.5	...	...
Sirius[a]	19.5 ± 1.5	19.6	11.3 ± 1.3	7.6 ± 3.0	$1.4^{+0.6}_{-1.4}$	17.23 ± 0.20	(1.6 ± 0.2)	1.6 ± 0.8	-0.60 ± 0.26
G191-B2B[c]	20.6	20.3	≈10.9	≈7.0	≈1.6	18.27	$1.4^{+0.1}_{-0.3}$	5.9	−1.22
G191-B2B[d]	9.9	20.3	≈12.4	≈9.0	≈2.5	17.60	$1.^{+0.4}_{-0.1}$	0.21	+0.09

[a] Component 1 (LIC).
[b] Average values for α Cen A and B assuming that D/H = 1.6×10^{-5}.
[c] Component B (LIC).
[d] Component A.

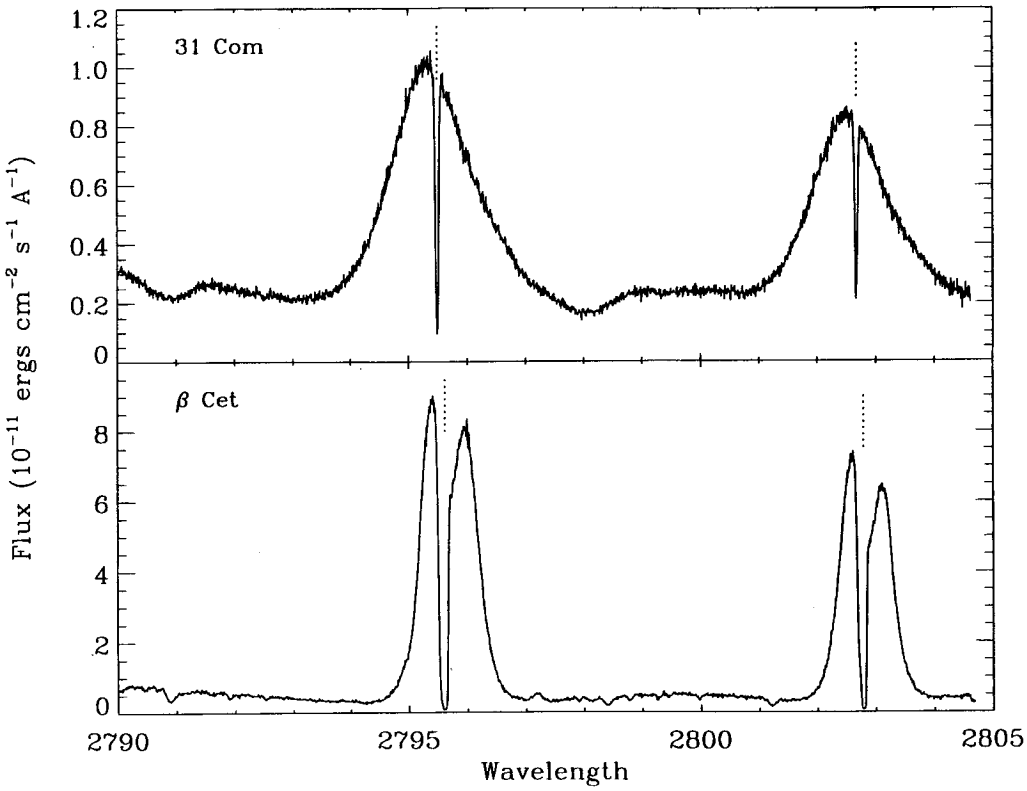

FIG. 4.—GHRS EB spectra of the Mg II *h* and *k* lines of 31 Com and β Cet. The positions of the interstellar Mg II absorption lines are indicated with vertical dotted lines.

Mg II spectra are shown in Figure 4, where the locations of the ISM absorption lines are identified with vertical dotted lines. We note that 31 Com ($l = 115°$, $b = +89°$) samples the line of sight to the north Galactic pole and β Cet ($l = 111°$, $b = -81°$) samples a line of sight near the south Galactic pole. Neither line of sight was previously studied with GHRS spectra.

The Mg II absorption lines seen toward β Cet are remarkably broad and deep. Close inspection of the cores of these features reveals that the absorption lines are not completely black. However, because the less optically thick *h* line does not show more residual flux in the absorption-line core than the more optically thick *k* line, we believe that the observed residual flux is due to scattered light and that both the *h* and *k* ISM absorption lines should be black at line center. Although scattered light is less of a problem for the EB grating than it is for the EA grating, some scattered light is expected for EB at roughly the level seen in the Mg II absorption-line cores of β Cet (Cardelli, Ebbets, & Savage 1990; Cardelli, Savage, & Ebbets 1991). We corrected for the scattered light by subtracting a flux of 6.0×10^{-13} ergs cm^{-2} s^{-1} Å^{-1} from the entire spectrum before fitting the absorption lines.

The Lyα lines of 31 Com, β Cet, and β Cas are displayed in Figure 5. These spectra all show broad interstellar H I absorption centered near 1215.7 Å and narrow interstellar D I absorption near 1215.35 Å. Geocoronal emission is also present in all these spectra and is marked in Figure 5 with dotted lines. For the β Cet and β Cas spectra, the geocoronal emission is well separated from the sides of the interstellar H I absorption lines, and can therefore be removed by fitting Gaussians to the emission and then subtracting the Gaussians from the data. For the 31 Com spectrum, we had to use a different technique to remove the geocoronal emission. We assumed that the interstellar H I absorption line is symmetric about the ISM flow velocity measured from the interstellar Mg II lines (see Fig. 4). We then simply reflected the bottom of the blue side of the absorption profile over to the red side of the absorption profile in order to correct for the geocoronal emission. The thick histogram in the 31 Com spectrum in Figure 5 shows the resulting profile.

For the 31 Com and β Cet spectra, there is no significant flux present in the cores of the H I absorption lines after the geocoronal emission is removed. For the β Cas spectrum, which is the only one obtained with the G140M grating, there appears to be some positive flux present that we attribute to scattered light. We removed this emission by subtracting a flux of 8.5×10^{-14} ergs cm^{-2} s^{-1} Å^{-1} from the data between 1215.1 and 1216.1 Å.

5. ANALYSIS OF THE LINE OF SIGHT TOWARD 31 COM

Our fits to the Mg II absorption lines for the 31 Com line of sight are shown in Figure 6. Polynomials were used to estimate the shape of the stellar Mg II emission line above the interstellar absorption. The dotted lines in the figure are the absorption lines before instrumental broadening, and the thick solid lines are after instrumental broadening. The data are very well fitted by a single absorption component. The two Mg II lines were modeled separately. Random errors were estimated for each fit by using Monte Carlo techniques. We then averaged the fit parameters measured for the two Mg II lines to produce the interstellar Mg II parameters and 1 σ errors listed in Table 2. This table lists the central velocity, Doppler width parameter ($b_{\rm Mg\,II}$), and logarithmic Mg II column density (log $N_{\rm Mg\,II}$) for the 31 Com line of sight. The reduced χ^2-value (χ^2_ν) for the Mg II fits is also listed.

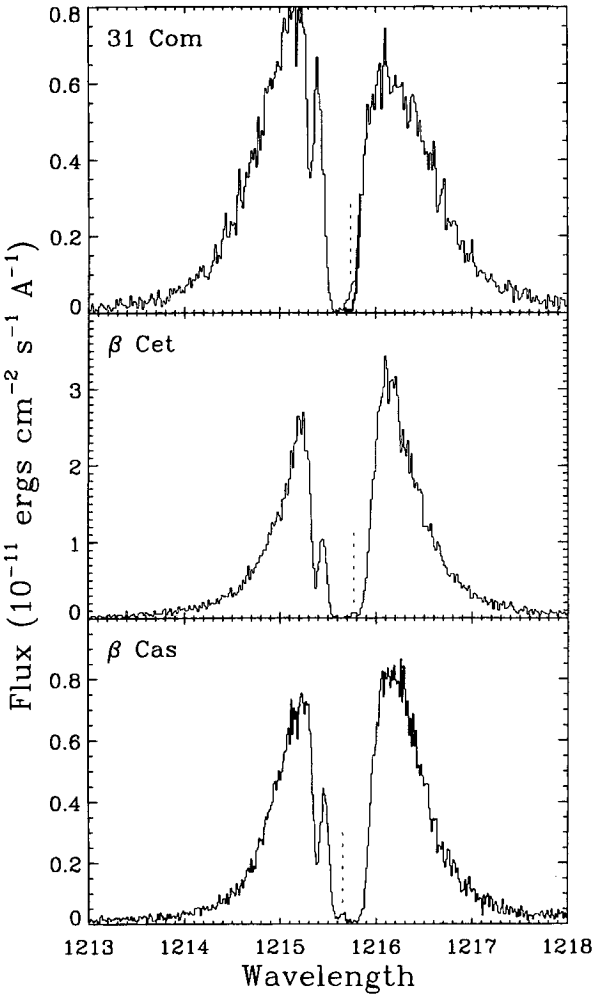

FIG. 5.—Moderate-resolution GHRS spectra of the Lyα lines of 31 Com, β Cet, and β Cas, showing interstellar H I absorption near 1215.7 Å and interstellar D I absorption near 1215.35 Å. Geocoronal emission is marked with vertical dotted lines. For 31 Com, we show the H I absorption profile, after correcting for the geocoronal emission, as a thick solid histogram.

When we compare the Mg II *k* and Lyα lines of 31 Com, as we have just done for HR 1099, we also find excellent agreement between the two profiles, at least for the parts of the profiles uncontaminated by interstellar absorption.

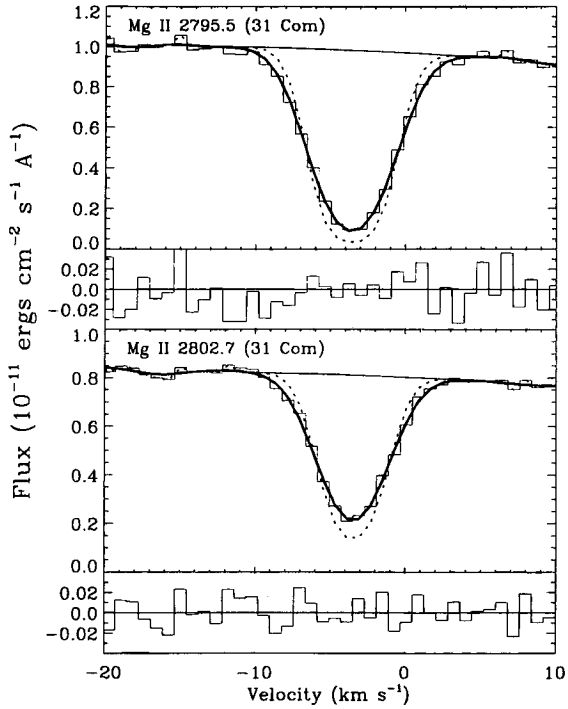

FIG. 6.—Fits to the interstellar Mg II absorption lines observed toward 31 Com, with the residuals shown below the fits. The dotted lines and the thick solid lines are the fits before and after convolution with the instrumental profile, respectively.

Thus, in our analysis of the interstellar H I and D I absorption lines seen toward 31 Com, we use the Mg II *k* line shape as our initial model for the intrinsic stellar Lyα profile. After altering this profile slightly to maximize the quality of our fit, we obtain the fit shown in Figure 7*b*. For this model, and for all our other fits to the Lyα lines of 31 Com, β Cet, and β Cas, we require the D I line to have the same velocity as the H I line, and we force $b_{\rm D\,I} = b_{\rm H\,I}/2^{1/2}$. This relation is exactly true when there is no nonthermal broadening (i.e., $\xi = 0$ km s^{-1}), which should be a good approximation because the H I and D I lines analyzed in Papers I–IV were found to be dominated by thermal broadening. The parameters of the fit in Figure 7*b* are given in Table 4, along with the parameters of all our other fits to the Lyα lines of 31 Com, β Cet, and β Cas, which will be described below. The errors listed in

TABLE 4

PARAMETERS FOR POSSIBLE MODELS OF INTERSTELLAR ABSORPTION COMPONENTS

Star	Figure	Velocity (km s^{-1})	$b_{\rm H\,I}$ (km s^{-1})	log $N_{\rm H\,I}$	D/H (10^{-5})	χ^2_ν
31 Com.....	7*a*	−3.7 ± 0.4	12.5 ± 0.3	17.778 ± 0.025	2.0 ± 0.3	1.027
31 Com.....	7*b*	−3.9 ± 0.4	11.8 ± 0.3	17.881 ± 0.017	1.6 ± 0.2	0.923
31 Com.....	7*c*	−4.0 ± 0.4	5.7 ± 1.9	18.154 ± 0.010	1.5 ± 0.9	1.164
β Cet	10*a*	9.1 ± 0.3	12.7 ± 0.5	(18.200)	2.9 ± 0.2	1.257
		(1.6)	16.8 ± 0.3	(16.623)	(2.9)	1.257
β Cet	10*b*	7.2 ± 0.4	9.7 ± 1.4	18.388 ± 0.007	2.1 ± 1.0	1.057
		(−0.3)	13.8 ± 0.7	(16.811)	(2.1)	1.057
β Cet	10*c*	7.6 ± 0.5	6.9 ± 1.1	18.477 ± 0.006	4.1 ± 2.4	1.134
		(0.1)	13.3 ± 1.0	(16.901)	(4.1)	1.134
β Cet	11	6.5 ± 0.3	11.3 ± 0.7	18.388 ± 0.007	1.5 ± 0.2	1.103
		(0.8)	(11.3)	(16.568)	(1.5)	1.103
		(−2.9)	(11.3)	(16.469)	(1.5)	1.103
β Cas	12*a*	11.0 ± 0.2	13.9 ± 0.1	(18.000)	2.5 ± 0.1	1.551
β Cas	12*b*	10.2 ± 0.2	11.2 ± 0.4	18.231 ± 0.007	1.3 ± 0.1	1.010
β Cas	12*c*	10.2 ± 0.2	8.7 ± 0.9	18.343 ± 0.006	1.1 ± 0.3	1.505

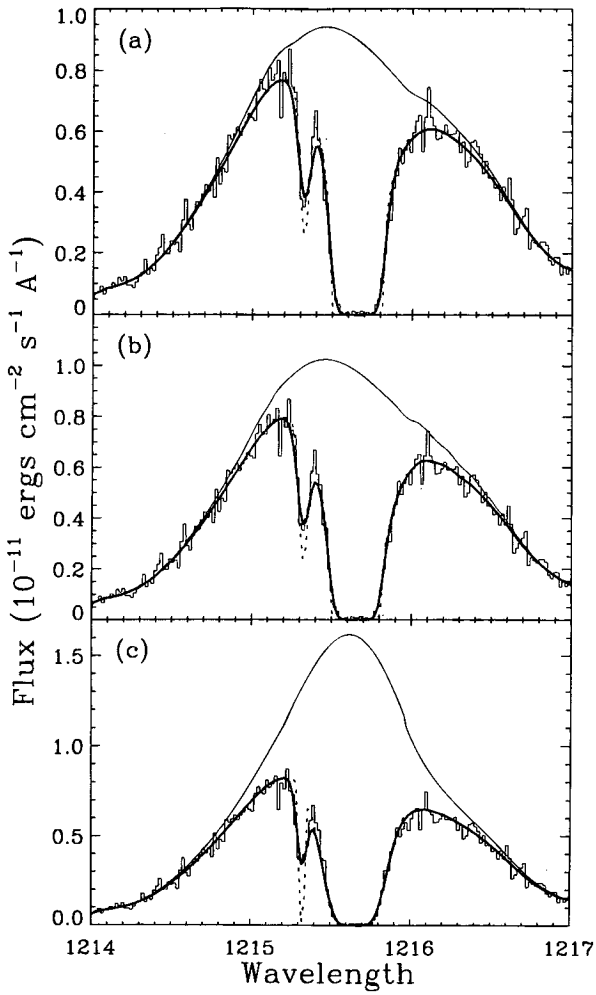

FIG. 7.—Three fits to the interstellar H I and D I absorption lines observed toward 31 Com, with an increasing value of the measured H I column density from (*a*) to (*c*). The dotted lines and the thick solid lines are the fits before and after convolution with the instrumental profile, respectively.

Table 4 are the 1 σ random errors of our measurements, which have been computed by using Monte Carlo techniques.

Although the assumed stellar Lyα profile in Figure 7*b* appears to be a fairly accurate representation of the real profile, it is important to recognize that one does not have to alter this profile very much to obtain significantly different model parameters, especially because interstellar absorption lines are generally not fully resolved in moderate-resolution GHRS spectra and the interstellar H I optical depth is $\sim 10^5$. Thus, in our analysis of the Lyα lines of 31 Com, β Cet, and β Cas, we experimented with stellar line profiles that have been altered from our initial model profiles, and some of the fits resulting from these experiments are presented here. This approach will allow us to estimate the systematic errors introduced into our analysis by uncertainties in the intrinsic stellar emission line profiles.

For 31 Com, Figure 7*a* shows a stellar Lyα profile that results in a model with an interstellar H I column density lower than that computed in our initial model shown in Figure 7*b*. The parameters for these fits are given in Table 4. Figure 7*c* shows a stellar Lyα profile that produces a fit to the data with a higher H I column density. The models shown in Figures 7*a* and 7*c* are both fairly good fits to the data, but these models and the assumed stellar profiles have problems that lead us to consider these models unacceptable.

Considering first the fit to the data shown in Figure 7*a*, we note that the H I Doppler parameter of this model (12.5 ± 0.3 km s^{-1}) is higher than the Doppler parameter of our initial model (11.8 ± 0.3 km s^{-1}; see Table 4). This is because both the Doppler parameter and the column density play a role in broadening the H I absorption line: since the column density of the model in Figure 7*a* is lower than our initial model, the Doppler parameter must be increased to a value larger than that of our initial model in order to produce an H I absorption line that is broad enough to match the data. However, the Doppler parameter suggested by the model in Figure 7*a* is inconsistent with the Mg II Doppler parameter ($b_{\rm Mg\,II} = 2.39 \pm 0.10$ km s^{-1}). The Mg II Doppler parameter suggests a maximum temperature of about 9100 K, but the H I Doppler parameter of the model in Figure 7*a* suggests a temperature of about 9500 K, assuming that the nonthermal broadening, ξ, is 0 km s^{-1}. (Note that assuming $\xi > 0$ km s^{-1} only makes the discrepancy larger.) We consider the model in Figure 7*a* to be unacceptable, and we consider log $N_{\rm H\,I} = 17.778$ to be a lower limit to the actual column density.

In order to produce a model with a larger H I column density than that shown in Figure 7*b*, $b_{\rm H\,I}$ must be decreased in order to prevent the H I absorption from becoming too broad. For the model shown in Figure 7*c*, $b_{\rm H\,I}$ has been decreased to only 5.7 ± 1.9 km s^{-1}, which suggests a temperature no higher than 3500 K and probably lower than 2000 K. This is a very suspicious result, considering that the lowest LISM temperature ever measured for any line of sight toward a nearby star is $T = 5400 \pm 500$ K for the α Cen line of sight (see Paper III). The Mg II Doppler parameter for the 31 Com line of sight does not indicate unusually low temperatures, so we consider the LISM temperature implied by the fit in Figure 7*c* to be unreasonable and therefore consider the fit unacceptable.

Considering the fits in Figure 7 (and others not presented), we use the type of reasoning expressed in the previous two paragraphs to derive our best estimates of the ISM parameters and their errors for the 31 Com line of sight. These final results, which will be discussed in detail in § 8, are presented in Table 3.

6. ANALYSIS OF THE LINE OF SIGHT TOWARD β CET

The interstellar Mg II absorption lines observed toward β Cet are shown in Figure 8. The obviously asymmetric appearance of these lines requires that more than one absorption component be present. A two-component fit is shown in the figure. In order to maximize the accuracy of the fit, we have fitted the *h* and *k* lines simultaneously. The parameters of the two-component model are listed in Table 2. The primary component is located at a velocity (9.1 ± 0.1 km s^{-1}) consistent with the velocity predicted for this line of sight by the LIC flow vector (8.2 km s^{-1}). This component also has a Doppler parameter that is very similar to Mg II Doppler parameters measured for other lines of sight through the LIC, including that measured toward 31 Com.

However, the column density of this LIC component (log $N_{\rm Mg\,II} = 14.245 \pm 0.104$) is remarkably high, well over an order of magnitude larger than any other Mg II column density measured from GHRS data for a line of sight

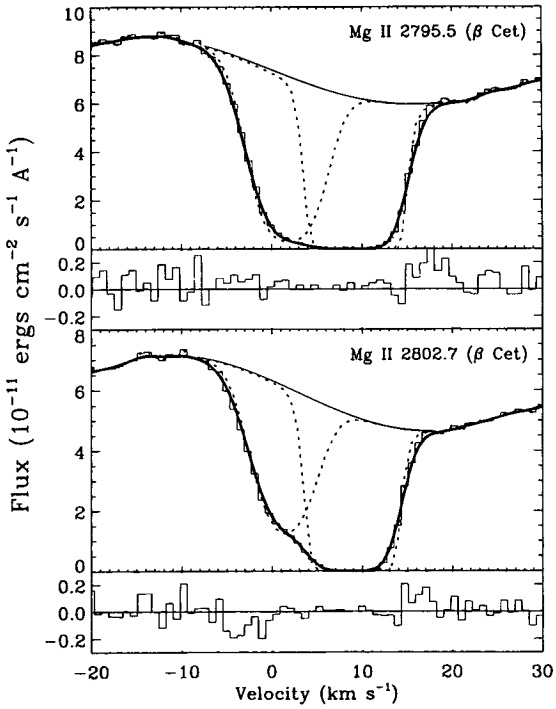

FIG. 8.—Two-component fits to the interstellar Mg II absorption lines observed toward β Cet, with the residuals shown below the fits. The dotted lines are the individual components, and the thick solid lines are the convolution of the sum of the components with the instrumental profile.

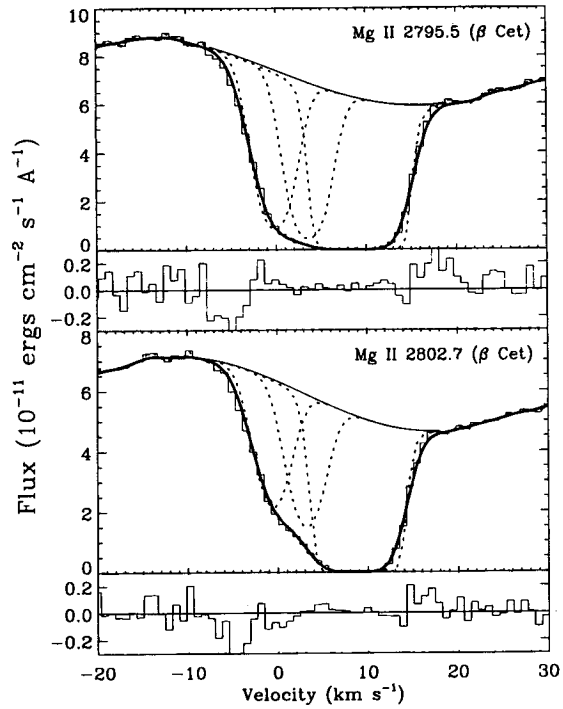

FIG. 9.—Three-component fits to the interstellar Mg II absorption lines observed toward β Cet, with the residuals shown below the fits. The dotted lines are the individual components, and the thick solid lines are the convolution of the sum of the components with the instrumental profile.

through the LIC. The problems this creates become evident only after the H I column density is measured (see § 8.4). We tried to reduce the total column density of our model by separating the primary component into two components. However, neither of the two resulting components was at the LIC velocity, both had Doppler parameters near 1.6 km s^{-1}, which is lower than any previously measured Mg II Doppler parameter, and the total column density was only reduced by a factor of 2. Thus, we do not consider this model to be an improvement over the fit in Figure 8.

The second component seen in Figure 8 has a suspiciously large Doppler parameter ($b_{\rm Mg\,II} = 3.71 \pm 0.10$ km s^{-1}). In Figure 9, we show that this component can be separated into two components that have the same Doppler parameters as the primary component. The parameters of this fit are also given in Table 2. Note that the parameters listed in parentheses in Tables 2–4 are fixed rather than derived parameters. For the three-component fit in Figure 9, we forced one of the components to have identical parameters to the primary component of the two-component fit in Figure 8, and we forced the Doppler parameters of the other two components to be the same as that of this primary component.

For our fit to the Lyα line of β Cet, we adopted, as our initial estimate for the intrinsic stellar profile, the Lyα profile used in Paper I for the G8 star of the Capella binary system. We do this because β Cet is considered to be very similar to Capella's G8 star in many ways (see, e.g., Ayres 1988). We initially used the two-component ISM model suggested by the Mg II fit in Figure 8 as a guide in producing an analogous two-component fit to the Lyα line. We assumed that the velocity separation between the two components is the same as in the fit in Figure 8, and we assume that the difference in H I column density is the same as the difference in Mg II column density. We also assumed that both components have the same D/H ratio. Our initial fit to the data is shown in Figure 10*b*. The H I and D I absorption from the primary interstellar component is shown as a dotted line in the figure, the absorption from the secondary component is shown as a dot-dashed line, and the combination of the two components is shown as a thick solid line. The parameters of the model are given in Table 4.

Figure 10 is analogous to Figure 7 in that we have altered the assumed stellar profile in order to obtain fits to the data with lower and higher derived H I column densities than our initial fit. These fits are shown in Figures 10*a* and 10*c*, and the parameters of these models are also given in Table 4. The stellar profile shown in Figure 10*a* was designed to produce a fit with the required value of log $N_{\rm H\,I} = 18.2$. The resulting model is a reasonable match for the data, but this model suffers from the same problem as the 31 Com fit in Figure 7*a*—the H I Doppler parameter of the primary component ($b_{\rm H\,I} = 12.7 \pm 0.5$ km s^{-1}) suggests an ISM temperature ($T \approx 9800$ K) that is too high when compared with the upper limit of $T < 9500$ K suggested by the Mg II Doppler parameter ($b_{\rm Mg\,II} = 2.46 \pm 0.08$ km s^{-1}). Thus, we do not consider the fit in Figure 10*a* to be acceptable, and we therefore consider 18.2 to be a lower limit for log $N_{\rm H\,I}$.

The fit in Figure 10*c* suffers from the same problem as the 31 Com fit in Figure 7*c*. The primary component's H I Doppler parameter is only $b_{\rm H\,I} = 6.9 \pm 1.1$ km s^{-1}, which suggests a temperature no higher than 3900 K and probably lower than 3000 K. We believe that this temperature probably is unreasonably low. Close inspection of the fit in Figure 10*c* reveals that the H I absorption of the model is still a bit broader than the data, despite the very low Doppler parameter. This problem becomes even more evident for models with even higher H I column densities

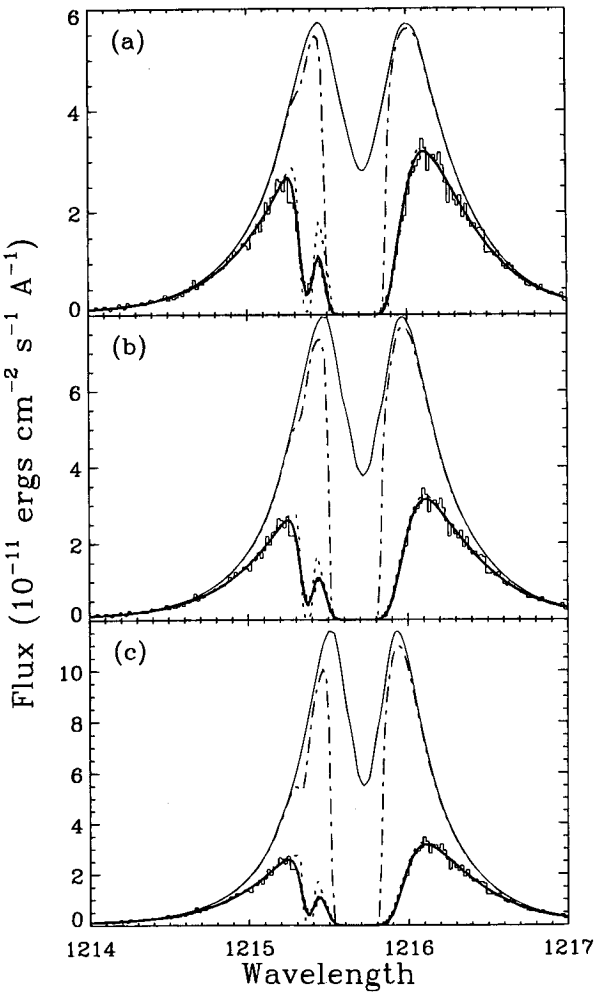

FIG. 10.—Three two-component fits to the interstellar H I and D I absorption lines observed toward β Cet, with an increasing value of the measured H I column density from (*a*) to (*c*). The dotted lines and dot-dashed lines are the two H I + D I absorption components, and the thick solid lines are the convolution of the sum of the components with the instrumental profile.

(and lower H I Doppler parameters). For all these reasons, we consider the model shown in Figure 10*c* to be only marginally acceptable at best.

The two-component models in Figure 10 are all based on the two-component fit to the Mg II lines in Figure 8. In Figure 11, we show a three-component fit to the Lyα line that is based on the three-component Mg II fit in Figure 9. The parameters of the model are given in Table 4. The velocity separations of the components and their relative column densities were required to be the same as those measured in the Mg II fit in Figure 9. We also forced the three components to have the same Doppler parameter, analogous to what was done for Mg II.

Based on the fits in Figures 8–11, we determine our best estimates for the parameters of the primary component (which represents matter in the LIC) and assign errors to these parameters. The final results are listed in Table 3. We also list the parameters of the second ISM component for the β Cet line of sight, assuming that the two-component model of Figures 8 and 10 is valid. The values and errors listed in Table 3 are discussed in detail in § 8, but we do note here the large uncertainty in the D/H ratio for the β Cet line of sight. The reason for this large error is evident from the large variation in the D/H ratio measured for the fits in Figures 10 and 11, and from the large random errors in the D/H ratio measured for the fits in Figures 10*b* and 10*c*. For all other lines of sight that have been analyzed by using GHRS data to date, the error in the D/H ratio has been dominated by the error in the H I column density rather than the D I column density. This is not true for the β Cet line of sight. It is not possible to determine the optical depth of the line accurately, because the D I absorption line is deep and not fully resolved in our G160M data. Since the D I lines of 31 Com and β Cas are not as deep, we can measure the optical depths and column densities for those lines more accurately, even though the lines are not fully resolved.

7. ANALYSIS OF THE LINE OF SIGHT TOWARD β CAS

We have no observations of the Mg II lines of β Cas, and there are no previously derived stellar Lyα profiles for a star with a spectral type similar to β Cas (F2 III–IV). Since we must start somewhere in order to analyze the interstellar H I and D I absorption lines of β Cas, we start with the profile used in Paper III for α Cen A (profile model 2A, to be exact), which is a G2 V star. The Wilson-Bappu effect (Wilson & Bappu 1957) is a strong correlation between the widths of chromospheric lines like Ca II, Mg II, and Lyα and the absolute stellar magnitude. The Mg II lines of β Cas are expected to be 65% broader than those of α Cen A, based on the Wilson-Bappu correlation of Vladilo et al. (1987). We assume that the same is true for Lyα and broaden the α Cen A Lyα profile by 65% before attempting our first fit to the Lyα line of β Cas. We found, however, that we had to alter this profile greatly in order to maximize the quality of the fit, and the resulting profile and our initial fit to the β Cas data are shown in Figure 12*b*.

Once again, we altered the assumed stellar profile to produce models with lower and higher H I column densities. These models are shown in Figures 12*a* and 12*c*, and the corresponding parameters are given in Table 4. The stellar profile shown in Figure 12*a* was designed to produce a model with log $N_{\rm H\,I} = 18.0$, and for the fit in Figure 12*a*, we have in fact forced log $N_{\rm H\,I}$ to be 18.0. However, the resulting fit is not a very good match for the data, because the sides of the H I absorption line are too steep. This problem becomes even more obvious for models with even lower H I column densities. Thus, we consider 18.0 to be a lower limit for log $N_{\rm H\,I}$. The model shown in Figure 12*c* is also not a particularly good match to the data because the H I absorption is too broad and the D I absorption is noticeably narrower than the data. Thus, we believe the H I column density must be lower than the log $N_{\rm H\,I} = 18.343$ value measured from the fit in Figure 12*c*. The results of our β Cas analysis are summarized in Table 3, together with the results of the 31 Com and β Cet analyses.

8. DISCUSSION AND CONCLUSIONS

As mentioned in § 1, Papers III and IV showed that absorption from "hydrogen walls" surrounding the Sun and other stars may be contributing to the observed H I absorption. For the lines of sight analyzed in this paper, we were able to model the Lyα absorption without such an absorption component. This does not mean, however, that hydrogen wall absorption is not present. High-resolution Ech-A observations of Lyα are necessary to detect the small

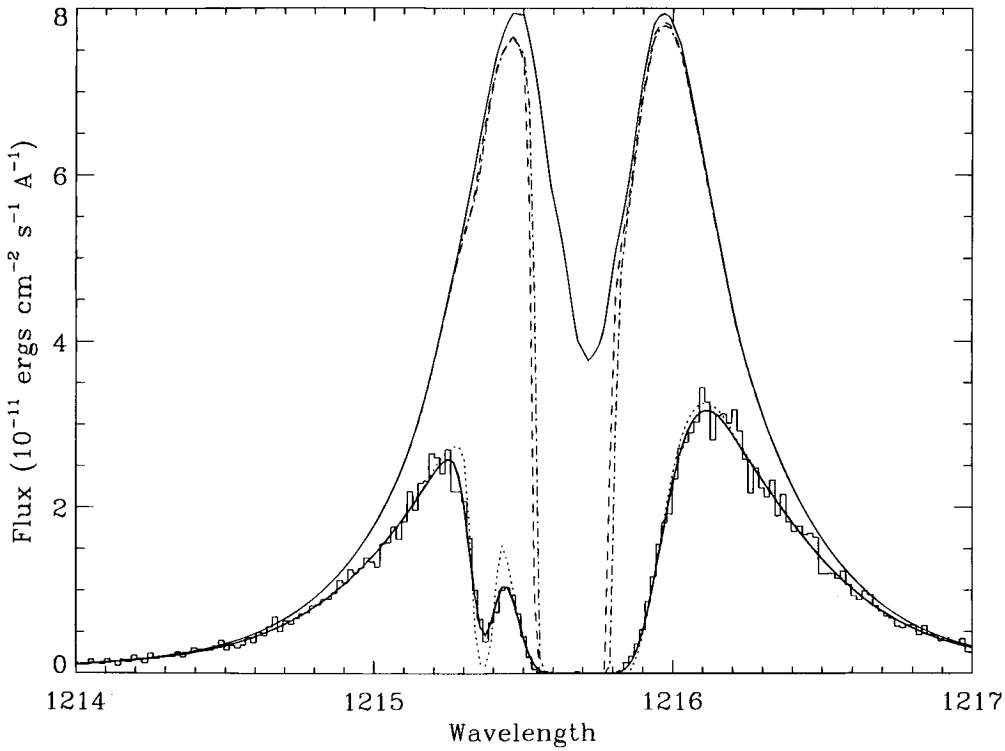

FIG. 11.—A three-component fit to the interstellar H I and D I absorption lines observed toward β Cet. The dotted, dashed, and dot-dashed lines are the three H I + D I absorption components, and the thick solid line is the convolution of the sum of the components with the instrumental profile.

temperature and velocity discrepancies between D I and H I used in Papers III and IV to infer the presence of the hydrogen walls. Since we have only moderate-resolution spectra for 31 Com, β Cet, and β Cas, we are unable to search for hydrogen wall absorption along these lines of sight. We do have an Ech-A observation of Lyα for HR 1099, but unfortunately the Mg II data suggest at least three interstellar components. Thus, our Lyα fit necessarily has a large number of free parameters, which will allow us to fit the data even if there is some absorption from an undetected hydrogen wall.

Since absorption from undetected hydrogen walls may be a significant source of systematic error in our analysis, it is useful to assess the possibility that this absorption is important. We define θ to be the angle between a line of sight and the upwind direction of the local interstellar flow vector (assumed to be the LIC vector from Lallement et al. 1995). For the lines of sight to HR 1099, 31 Com, β Cet, and β Cas, we compute $\theta = 155°$, 73°, 109°, and 112°, respectively. We now make several assertions relevant to the likelihood of there being contaminating hydrogen wall absorption in our data:

1. We would expect the solar hydrogen wall absorption to be most evident in upwind directions (e.g., $\theta < 90°$), because the density enhancement of the wall, and the velocity separation between the wall and ISM absorption, should be greatest in that direction. Only 31 Com lies in such a direction, but only marginally so with $\theta = 73°$. Since the redshift of warm H I in the wall is proportional to cos θ, it would be very difficult to detect solar hydrogen wall absorption even toward 31 Com.

2. The relatively large interstellar H I column density observed toward β Cet would make it difficult to detect any solar or stellar hydrogen wall absorption.

3. It is likely that HR 1099 and 31 Com lie in the hot ionized phase of the ISM, rather than inside warm neutral clouds like those that envelop the Sun (see § 8.5 below). Thus, it is unlikely that these stars are surrounded by neutral hydrogen walls.

Based on these considerations, we believe that our 31 Com data are the most vulnerable to contamination from solar hydrogen wall absorption, and that our β Cas data are the most susceptible to a stellar hydrogen wall absorption component. It is impossible to be more precise than this with the moderate-resolution data in hand.

Table 3 summarizes the results obtained in this paper concerning the lines of sight toward HR 1099, 31 Com, β Cet, and β Cas. We also list the results previously obtained in Papers I–IV concerning the lines of sight toward Capella, Procyon, α Cen (the average values for the two stars in the system), ϵ Ind, and λ And, as well as the results obtained for Sirius and G191-B2B by Lallement et al. (1994, 1995), Bertin et al. (1995), and Lemoine et al. (1996). For these last two stars, we list the components at the LIC velocity, and for G191-B2B we also list data for the 9.9 km s^{-1} component (component A). All quantities in parentheses are assumed values. The hydrogen column densities and the corresponding magnesium depletions for Sirius, Procyon, and α Cen are derived from the measured D I column densities and the assumed D/H ratio. The uncertainty in the assumed D/H ratio for these three stars was set to include the derived D/H ratios for all of the stars in the table, except for the very uncertain value for β Cet.

8.1. *Line-of-Sight Velocities*

Lallement & Bertin (1992) and Lallement et al. (1995) have found that nearly all lines of sight toward nearby stars show Mg II and Fe II absorption at velocities consistent

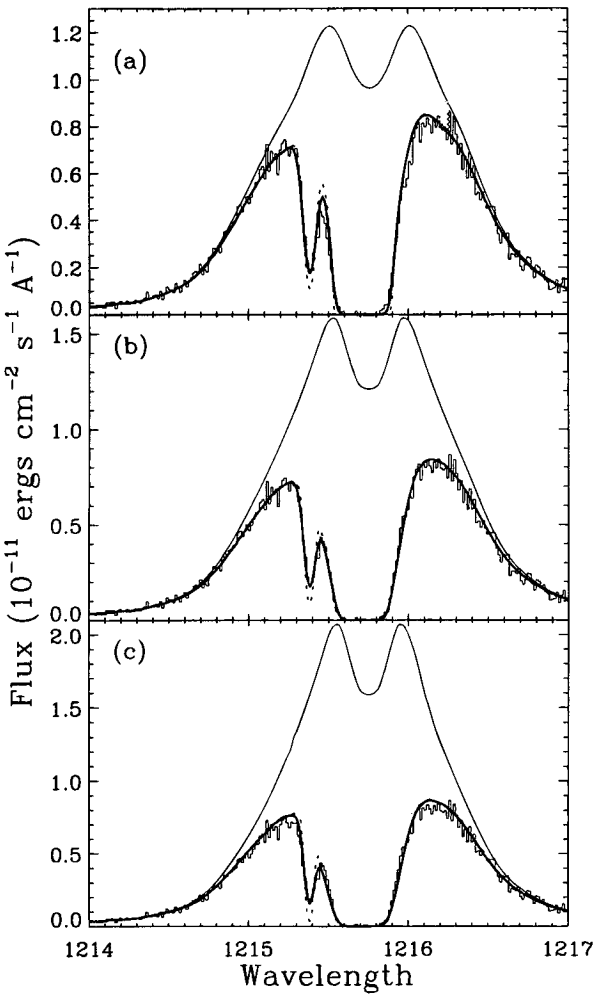

FIG. 12.—Three fits to the interstellar H I and D I absorption lines observed toward β Cas, with an increasing value of the measured H I column density from (*a*) to (*c*). The dotted lines and the thick solid lines are the fits before and after convolution with the instrumental profile, respectively.

with a flow vector in the heliocentric rest frame with a magnitude of 26 ± 1 km s^{-1} moving toward Galactic coordinates $l = 186° \pm 3°$ and $b = -16° \pm 3°$. The projected LIC flow vector velocities toward the stars of interest are listed in the third column of Table 3. These predictions indicate that the 21.9 ± 2 km s^{-1} component toward HR 1099, the 8 ± 2 km s^{-1} component toward β Cet, and the one known component at 10 ± 1 toward β Cas are formed in the LIC. However, the one observed component in the line of sight to 31 Com at -4 ± 1 km s^{-1} is inconsistent with the LIC projected velocity. Thus, the components with the largest column densities toward three of the four stars in our sample are consistent with the LIC flow vector.

Of the four stars studied in this paper, only 31 Com, the star located at the north Galactic pole, shows its main absorption at a velocity inconsistent with the LIC flow vector. The sample of stars used in deriving the LIC vector (Lallement et al. 1995) did not include any stars at high Galactic latitudes. One of the velocity components of β Leo ($l = 251°$, $b = +71°$, $d = 12.2$ pc) is possibly related to the LIC, but the velocity difference from the LIC ($+2.3$ km s^{-1}) is high. Since we find that the measured velocity toward 31 Com is 2.7 km s^{-1} relative to the projected LIC velocity, there is evidence that, at very high Galactic latitudes, either the LIC extends for only a very short distance (as suggested by Lallement et al. 1995), and another cloud provides nearly all of the interstellar absorption, or the LIC does not show rigid-body motion at these latitudes. On the other hand, β Cet located at $b = -81°$ shows absorption at the projected LIC velocity as does α PsA located at $b = -65°$, which Lallement et al. (1995) used to determine the LIC flow vector. Thus, the LIC flow vector appears to be valid for lines of sight near the south Galactic pole (but see § 8.4).

8.2. *Temperatures and Turbulent Velocities*

The inferred temperatures for the matter flowing with the LIC velocity vector toward nearly all of the stars listed in Table 3 are consistent with a temperature of about 7000 K. The only exceptions are ϵ Ind and λ And, stars for which we do not have Mg II or Fe II spectra and thus cannot determine whether there is more than one velocity component in the line of sight. The most accurately determined temperatures are for the Capella and Procyon lines of sight, for which the cited errors are a linear sum of random and systematic errors. Likewise, the turbulent velocities for the lines of sight through the LIC are consistent with ξ in the range 1.0–1.6 km s^{-1}. Thus, the LIC appears to have a small range of temperature and turbulent velocity.

8.3. D/H *Ratios*

The D/H ratios for the four stars in this study and the other stars listed in Table 3 are all consistent with the most accurately determined values toward nearby stars described in Papers I–IV. In particular, they are consistent with the value of D/H $= 1.60^{+0.14}_{-0.19} \times 10^{-5}$ toward Capella (Papers I and II) and D/H $= (1.6 \pm 0.4) \times 10^{-5}$ toward ϵ Ind (Paper IV). The value for Capella includes the cited random error of $\pm 0.09 \times 10^{-5}$ and the systematic error of $^{+0.05}_{-0.10} \times 10^{-5}$ due to the uncertain intrinsic stellar Lyα line profile shape. Thus, the evidence is increasing that there is a single value of the D/H ratio in the LISM with an uncertainty or range of less than 15%, although Lemoine et al. (1996) suggest that the D/H ratio in component A (9.9 km s^{-1}) toward G191-B2B may be slightly smaller than 1.6×10^{-5}. Detailed studies of additional lines of sight are needed to determine whether the D/H ratio varies in the LISM.

8.4. *Gas-Phase Abundance of* Mg

The analysis of Lallement et al. (1994) demonstrated that Mg II is the dominant ionization state of magnesium in the LISM. Our results show that the gas-phase abundance of Mg II varies considerably in the LISM. Table 3 lists the logarithmic depletions of Mg II, defined by $D(\mathrm{Mg}) = \log (N_{\mathrm{Mg\,II}}/N_{\mathrm{H\,I}}) - \log (\mathrm{Mg/H})_\odot$, where the solar abundance of magnesium is $\log (\mathrm{Mg/H})_\odot = -4.41$ (Anders & Grevesse 1989). Note that these depletion values assume that all hydrogen in the LISM is neutral. The ionization state of the LISM is highly uncertain, however, and it is possible that more than half of the hydrogen is ionized (see, e.g., Lallement et al. 1994), in which case the depletion values in Table 3 might be too large by 0.3 dex or more. We find that D(Mg) ranges from the overabundant value of 0.30 ± 0.15 toward β Cet to the very underabundant value of -1.44 ± 0.16 for the 14.8 km s^{-1} component toward HR 1099, which represents a variation of more than a factor of 50. The large variations in D(Mg) strongly imply that the very wide range in the D/Mg II ratio seen in Table 3 (from 0.35 ± 0.25 for β Cet to 10.5 ± 1.7 for the 14.8 km s^{-1}

component for HR 1099) is due to variations in Mg II rather than D I. This supports our conclusion that the D/H ratio is nearly constant in the LISM.

The D(Mg) values for gas moving with the LIC velocity vector lie in the range -0.90 ± 0.10 to -1.36 ± 0.15 for all lines of sight except for β Cet. The α Cen line of sight shows a significantly larger Mg II abundance, as indicated by the small D/Mg II ratio (1.2 ± 0.2) and small depletion D(Mg) $= -0.46 \pm 0.05$. Similar results are seen for the Fe II abundance (see Paper III). This result is consistent with α Cen lying inside a cloud (the G cloud of Lallement & Bertin 1992) with different properties than the cloud in which the Sun resides (the AG or LIC cloud; Lallement et al. 1995). Besides having higher metal abundances than the LIC, the G cloud also appears to have a slightly different flow vector (Lallement et al. 1995) and a lower temperature (Paper III) than the LIC.

Except for the β Cet line of sight toward the south Galactic pole, the depletion of Mg for all directions in the LIC is consistent with D(Mg) $= -1.1 \pm 0.2$, which is in the middle of the range (from -0.59 to -1.57) found by Sofia, Cardelli, & Savage (1994) for warm gas in longer lines of sight through the Galaxy. The much larger value of D(Mg) seen at the LIC velocity toward β Cet may indicate that there are one or more clouds with the same projected flow velocity as the LIC cloud along this line of sight, but with much larger Mg abundances. The 9.9 km s^{-1} cloud toward G191-B2B also shows essentially no Mg depletion.

The β Cet, α Cen, G191-B2B, and perhaps Sirius lines of sight demonstrate that metal abundances in the LISM are remarkably inhomogeneous, since the Mg abundance apparently varies by over an order of magnitude over distances of only a few parsecs. The cause of these variations is subject to interpretation, but perhaps for these lines of sight, the interstellar gas has been shocked recently, removing magnesium atoms from dust grains and increasing the Mg abundance relative to other lines of sight.

8.5. *The Small Hydrogen Column Density toward the North Galactic Pole*

Despite the 80 pc line of sight, the hydrogen column toward 31 Com is only $\log N_{\rm H\,I} = 17.95 \pm 0.15$, corresponding to a mean hydrogen density $\langle n_{\rm H\,I} \rangle = 0.0034$ cm^{-3}. Since the mean hydrogen density toward 31 Com is roughly a factor of 30 smaller than in the solar environment, most of the line of sight toward 31 Com is essentially devoid of neutral hydrogen and probably contains hot low-density gas. The analysis of the *EUVE* spectra of the hot white dwarfs HZ 43 and GD 153, which are located at about 65 pc at similar Galactic latitude $b = 84°$, provides hydrogen column densities (Dupuis et al. 1995) that are similar to that toward 31 Com. Thus, the line of sight toward the north Galactic pole appears to be a low hydrogen column density patch in the sky, like the "interstellar tunnel" toward ϵ CMa (Gry et al. 1995; Welsh 1991). We note that the mean hydrogen density toward HR 1099 is also very low ($\langle n_{\rm H\,I} \rangle = 0.012$ cm^{-3}). At a distance of 36 pc, HR 1099 probably lies well outside the local neutral cloud, and the low H I column density suggests that HR 1099, like 31 Com, probably lies within the hot ionized phase of the ISM.

This work is supported by NASA grant S-56460-D to the National Institute of Standards and Technology, by NASA grants GO-5323.01-93A, GO-06067.01-94A, and NAGW-4529 to the University of Colorado, and by NASA grant GO-4447.03-92A to the Computer Sciences Corporation. We thank the referee for his useful comments.

REFERENCES

Anders, E., & Grevesse, N. 1989, Geochim. Cosmochim. Acta, 53, 197
Ayres, T. R. 1988, ApJ, 331, 467
Ayres, T. R., Brown, A., Gayley, K. G., & Linsky, J. L. 1993, ApJ, 402, 710
Ayres, T. R., & Linsky, J. L. 1982, ApJ, 254, 168
Bevington, P. R., & Robinson, D. K. 1992, Data Reduction and Error Analysis for the Physical Sciences (2d ed.; New York: McGraw-Hill)
Baranov, V. B., & Malama, Y. G. 1995, J. Geophys. Res., 100(A8), 14755
Bertin, P., Vidal-Madjar, A., Lallement, R., Ferlet, R., & Lemoine, M. 1995, A&A, 302, 889
Brandt, J. C., et al. 1994, PASP, 106, 890
Cardelli, J. A., Ebbets, D. C., & Savage, B. D. 1990, ApJ, 365, 789
Cardelli, J. A., Savage, B. D., & Ebbets, D. C. 1991, ApJ, 383, L23
Dempsey, R. C., Linsky, J. L., Fleming, T. A., & Schmitt, J. H. M. M. 1993, ApJS, 86, 599
Dempsey, R. C., Neff, J. E., Thorpe, M. J., Linsky, J. L., Brown, A., Cutispoto, G., & Rodonò, M. 1996, ApJ, 470, 1174
Donati, J.-F., Braun, S. F., Semel, M., Rees, D. E., Dempsey, R. C., Matthews, J. M., Henry, G. W., & Hall, D. S. 1992, A&A, 265, 682
Dupuis, J., Vennes, S., Bowyer, S., Pradhan, A. K., & Thejll, P. 1995, ApJ, 455, 574
Ferlet, R., Lecavelier, A., Vidal-Madjar, A., Bertin, P., Deleuil, M., Gry, C., Lagrange-Henry, A.-M., & Lallement, R. 1995, A&A, 297, L5
Gry, C., Lemonon, L., Vidal-Madjar, A., Lemoine, M., & Ferlet, R. 1995, A&A, 302, 497
Heap, S. R., et al. 1995, PASP, 107, 871
Henry, G. W., Eaton, J. A., Hamer, J., & Hall, D. S. 1995, ApJS, 97, 513
Lallement, R., & Bertin, P. 1992, A&A, 266, 479
Lallement, R., Bertin, P., Ferlet, R., Vidal-Madjar, A., & Bertaux, J. L. 1994, A&A, 286, 898
Lallement, R., Ferlet, R., Lagrange, A. M., Lemoine, M., & Vidal-Madjar, A. 1995, A&A, 304, 461
Lemoine, M., Vidal-Madjar, A., Bertin, P., Ferlet, R., Gry, C., & Lallement, R. 1996, A&A, 308, 601
Linsky, J. L., et al. 1993, ApJ, 402, 694 (Paper I)
Linsky, J. L., Diplas, A., Wood, B. E., Brown, A., Ayres, T. R., & Savage, B. D. 1995, ApJ, 451, 335 (Paper II)
Linsky, J. L., Piskunov, N., & Wood, B. E. 1996, Science, submitted
Linsky, J. L., & Wood, B. E. 1996, ApJ, 463, 254 (Paper III)
Neff, J. E., Landsman, W. B., Bookbinder, J. A., & Linsky, J. L. 1990, in Evolution in Astrophysics (SP-310; Paris: ESA), 341
Ockham, William of, ca. 1320, Quodlibeta Septem
Pauls, H. L., Zank, G. P., & Williams, L. L. 1995, J. Geophys. Res., 100, 21595
Robinson, R. D., Blackwell, J., Feggans, K., Lindler, D., Norman, D., & Shore, S. N. 1992, A User's Guide to the GHRS Software, Version 2.0 (Greenbelt: GSFC)
Soderblom, D. R., Hulbert, S. J., Leitherer, C., & Sherbert, L. E. 1994, *HST* Goddard High-Resolution Spectrograph Instrument Handbook, Version 5.0 (Baltimore: STScI)
Sofia, U. J., Cardelli, J. A., & Savage, B. D. 1994, ApJ, 430, 650
Strassmeier, K. G., Hall, D. S., Fekel, F. C., & Scheck, M. 1993, A&AS, 100, 173
Vladilo, G., Molaro, P., Crivellari, L., Foing, B. H., Beckerman, J. E., & Genova, R. 1987, A&A, 185, 233
Vogt, S. S. 1988, in The Impact of Very High S/N Spectroscopy on Stellar Physics, ed. G. Cayrel & M. Spite (Dordrecht: Kluwer), 253
Welsh, B. Y. 1991, ApJ, 373, 556
Williams, L. L., Hall, D. T., Pauls, H. L., & Zank, G. P. 1997, ApJ, in press
Wilson, O. C., & Bappu, M. K. V. 1957, ApJ, 125, 661
Wood, B. E., Alexander, W. R., & Linsky, J. L. 1996a, ApJ, 470, 1159 (Paper IV)
Wood, B. E., Harper, G. M., Linsky, J. L., & Dempsey, R. C. 1996b, ApJ, 458, 761